Label-free optical imaging of membrane patches for atomic force microscopy

Allison B. Churnside,[1,2] Gavin M. King,[1,3] and Thomas T. Perkins[1,4,*]

[1]*JILA, National Institute of Standards and Technology and University of Colorado, Boulder, Colorado 80309, USA*
[2]*Department of Physics, University of Colorado, Boulder, Colorado 80309, USA*
[3]*Currently with Department of Physics & Astronomy and Department of Biochemistry, University of Missouri, Columbia, Missouri 65211, USA*
[4]*Department of Molecular, Cellular, and Developmental Biology, University of Colorado, Boulder, Colorado 80309, USA*
**tperkins@jila.colorado.edu*

Abstract: In atomic force microscopy (AFM), finding sparsely distributed regions of interest can be difficult and time-consuming. Typically, the tip is scanned until the desired object is located. This process can mechanically or chemically degrade the tip, as well as damage fragile biological samples. Protein assemblies can be detected using the back-scattered light from a focused laser beam. We previously used back-scattered light from a pair of laser foci to stabilize an AFM. In the present work, we integrate these techniques to optically image patches of purple membranes prior to AFM investigation. These rapidly acquired optical images were aligned to the subsequent AFM images to ~40 nm, since the tip position was aligned to the optical axis of the imaging laser. Thus, this label-free imaging efficiently locates sparsely distributed protein assemblies for subsequent AFM study while simultaneously minimizing degradation of the tip and the sample.

OCIS codes: (180.0180) Microscopy; (180.5810) Scanning microscopy; (170.3880) Medical and biological imaging; (180.3170) Interference microscopy.

References and links

1. G. Binnig, C. F. Quate, and C. Gerber, "Atomic force microscope," Phys. Rev. Lett. **56**(9), 930–933 (1986).
2. M. Rief, M. Gautel, F. Oesterhelt, J. M. Fernandez, and H. E. Gaub, "Reversible unfolding of individual titin immunoglobulin domains by AFM," Science **276**(5315), 1109–1112 (1997).
3. S. Scheuring, and J. N. Sturgis, "Chromatic adaptation of photosynthetic membranes," Science **309**(5733), 484–487 (2005).
4. C. D. Frisbie, L. F. Rozsnyai, A. Noy, M. S. Wrighton, and C. M. Lieber, "Functional group imaging by chemical force microscopy," Science **265**(5181), 2071–2074 (1994).
5. F. Oesterhelt, D. Oesterhelt, M. Pfeiffer, A. Engel, H. E. Gaub, and D. J. Müller, "Unfolding pathways of individual bacteriorhodopsins," Science **288**(5463), 143–146 (2000).
6. S. M. Block, K. A. Fahrner, and H. C. Berg, "Visualization of bacterial flagella by video-enhanced light microscopy," J. Bacteriol. **173**(2), 933–936 (1991).
7. R. A. Lugmaier, T. Hugel, M. Benoit, and H. E. Gaub, "Phase contrast and DIC illumination for AFM hybrids," Ultramicroscopy **104**(3-4), 255–260 (2005).
8. A. Yildiz, J. N. Forkey, S. A. McKinney, T. Ha, Y. E. Goldman, and P. R. Selvin, "Myosin V walks hand-over-hand: single fluorophore imaging with 1.5-nm localization," Science **300**(5628), 2061–2065 (2003).
9. H. Yamada, H. Tokumoto, S. Akamine, K. Fukuzawa, and H. Kuwano, "Imaging of organic molecular films using a scanning near-field optical microscope combined with an atomic force microscope," J. Vac. Sci. Technol. B **14**(2), 812–815 (1996).
10. C. A. J. Putman, H. G. Hansma, H. E. Gaub, and P. K. Hansma, "Polymerized Lb Films Imaged with a Combined Atomic Force Microscope Fluorescence Microscope," Langmuir **8**(12), 3014–3019 (1992).
11. A. B. Mathur, G. A. Truskey, and W. M. Reichert, "Atomic force and total internal reflection fluorescence microscopy for the study of force transmission in endothelial cells," Biophys. J. **78**(4), 1725–1735 (2000).
12. H. Gumpp, S. W. Stahl, M. Strackharn, E. M. Puchner, and H. E. Gaub, "Ultrastable combined atomic force and total internal reflection fluorescence microscope [corrected]," Rev. Sci. Instrum. **80**(6), 063704 (2009).

#133107 - $15.00 USD Received 9 Aug 2010; revised 15 Oct 2010; accepted 26 Oct 2010; published 29 Oct 2010

13. H. Ewers, V. Jacobsen, E. Klotzsch, A. E. Smith, A. Helenius, and V. Sandoghdar, "Label-free optical detection and tracking of single virions bound to their receptors in supported membrane bilayers," Nano Lett. **7**(8), 2263–2266 (2007).
14. V. Jacobsen, P. Stoller, C. Brunner, V. Vogel, and V. Sandoghdar, "Interferometric optical detection and tracking of very small gold nanoparticles at a water-glass interface," Opt. Express **14**(1), 405–414 (2006).
15. A. R. Carter, G. M. King, and T. T. Perkins, "Back-scattered detection provides atomic-scale localization precision, stability, and registration in 3D," Opt. Express **15**(20), 13434–13445 (2007).
16. G. M. King, A. R. Carter, A. B. Churnside, L. S. Eberle, and T. T. Perkins, "Ultrastable atomic force microscopy: atomic-scale lateral stability and registration in ambient condition," Nano Lett. **9**(4), 1451–1456 (2009).
17. A. R. Carter, G. M. King, T. A. Ulrich, W. Halsey, D. Alchenberger, and T. T. Perkins, "Stabilization of an optical microscope to 0.1 nm in three dimensions," Appl. Opt. **46**(3), 421–427 (2007).
18. G. Meyer, and N. M. Amer, "Novel Optical Approach to Atomic Force Microscopy," Appl. Phys. Lett. **53**(12), 1045–1047 (1988).
19. R. P. Gonçalves, G. Agnus, P. Sens, C. Houssin, B. Bartenlian, and S. Scheuring, "Two-chamber AFM: probing membrane proteins separating two aqueous compartments," Nat. Methods **3**(12), 1007–1012 (2006).
20. D. J. Müller, and A. Engel, "Atomic force microscopy and spectroscopy of native membrane proteins," Nat. Protoc. **2**(9), 2191–2197 (2007).
21. Y. Shichida, S. Matuoka, Y. Hidaka, and T. Yoshizawa, "Absorption spectra of intermediate of bacteriorhodopsin measured by laser photolysis at room temperatures," Biochim. Biophys. Acta **723**(2), 240–246 (1983).
22. D. J. Müller, and A. Engel, "The height of biomolecules measured with the atomic force microscope depends on electrostatic interactions," Biophys. J. **73**(3), 1633–1644 (1997).
23. D. J. Griffiths, *Introduction to Electrodynamics* (Prentice Hall, Upper Saddle River, NJ, 1999).
24. A. Lukács, G. Garab, and E. Papp, "Measurement of the optical parameters of purple membrane and plant light-harvesting complex films with optical waveguide lightmode spectroscopy," Biosens. Bioelectron. **21**(8), 1606–1612 (2006).
25. H. Michel, and D. Oesterhelt, "Three-dimensional crystals of membrane proteins: bacteriorhodopsin," Proc. Natl. Acad. Sci. U.S.A. **77**(3), 1283–1285 (1980).

1. Introduction

The atomic force microscope (AFM) [1] has emerged as an increasingly important instrument for characterizing biological molecules [2,3]. At its core, an AFM consists of an atomically-sharp tip interacting with a sample. In biological applications of AFM, the sample is often prepared by allowing molecules of interest to adsorb randomly onto the surface. The user then images over a large area to find a desirable region for detailed study. Unfortunately, this process risks damage to the tip and the sample. Mechanical wear or adsorption of surface-bound proteins to the tip can degrade the tip's imaging capability. Moreover, alteration of the tip's chemical specificity by unwanted modification hinders chemical force microscopy [4] and coupling of biomolecules to the tip via covalent linkages [5]. Finally, the high scan rates typically used for large-area imaging can damage delicate biological samples due to decreased force control. Thus, while AFM-based studies clearly require tip-sample interactions, minimizing or even eliminating tip-sample interactions while locating biological samples for detailed study is desirable.

Small protein structures and even single proteins can be detected using wide field optical microscopy. For instance, video-enhanced differential interference contrast (DIC) microscopy can detect bacterial flagella [6], which are tubular protein assemblies with an outer diameter of 15 nm. Unfortunately, DIC microscopy is challenging to incorporate with AFM [7]. Fluorescence microscopy, which is quite compatible with AFM, has located single fluorescently labeled proteins with nanometer-scale precision [8]. Researchers have integrated fluorescent imaging into AFM, including AFM tips with an embedded microphotodetector [9] as well as AFMs combined with wide field [10] and total internal reflection [11,12] excitation.

Notwithstanding these successes, it is desirable to locate biomolecules without the need for fluorescence. Such label-free detection offers many advantages [13], most notably the use of native (or unmodified) proteins. Recently, label-free detection based on scanning the sample through a focused laser, called iSCAT [14], imaged both microtubules and virons (dia. = 45 nm) by detecting the back-scattered light [13]. We previously used back-scattered light

#133107 - $15.00 USD Received 9 Aug 2010; revised 15 Oct 2010; accepted 26 Oct 2010; published 29 Oct 2010

[15] to detect and thereby control the position of an AFM tip to achieve an ultrastable AFM [16]. The similarity between the optics used for label-free detection and our stabilized AFM suggested a tip-free means to optically image a sample prior to AFM-based studies.

In this report, we demonstrate the integration of label-free optical imaging of biological samples with AFM. The efficient optical imaging over a large area (30 × 30 μm^2) allowed us to select regions containing purple membrane patches for study with AFM (Fig. 1). Crucially, the optical image was inherently spatially aligned (or registered) to the subsequent AFM images with nanometer-scale precision (~40 nm). Further, it was sensitive, detecting ~8-nm tall patches of purple membrane, bacteriorhodopsin (BR) embedded in a lipid bilayer, with a high signal-to-noise ratio (S/N ≈20). This registration arises because both imaging modes share a common reference frame; the optical axis of the laser used for optical imaging is also used for aligning the tip. Thus, label-free optical imaging of biological samples prior to AFM investigation provides a means for increased reliability and performance in AFM by locating sparsely distributed biological samples while preserving the sharpness and chemical specificity of tips for high resolution imaging and force spectroscopy applications.

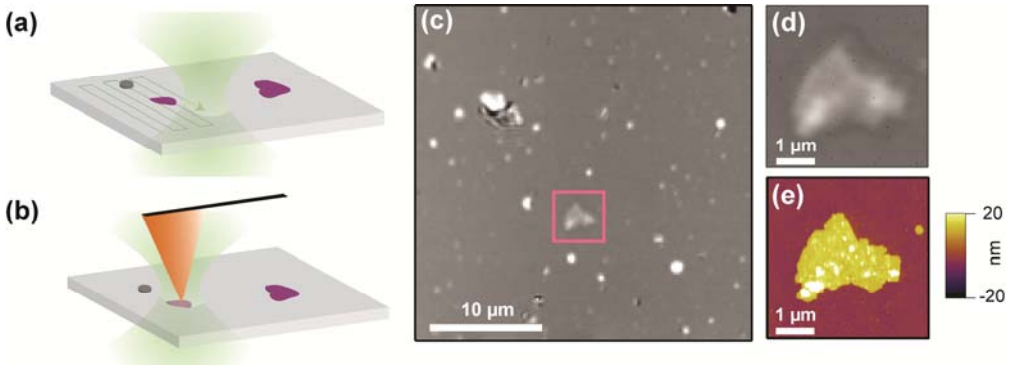

Fig. 1. Optically locating a region of interest for study by AFM. (a) With the tip retracted far from the surface, the sample is raster-scanned through the focused laser beam to obtain an image. (b) An AFM tip, aligned to the laser used for imaging, can probe an optically identified feature for detailed study. (c) A representative 30 × 30 μm^2 optical image (pixel size = 150 nm) revealed several surface features. The pink box denotes a purple membrane patch suitable for further study. (d) An optical image of area in the pink box (pixel size = 20 nm). (e) An AFM image of the same area shows it to be a purple membrane patch (pixel size = 4.2 nm).

2. Materials and methods

2.1 Experimental apparatus

The apparatus used for these experiments (Fig. 2) was an AFM designed and built in-house mounted on a research grade optical microscope enhanced for mechanical stability. A detailed discussion of the optics and instrumentation required for 3D back-scattered optical detection has previously been published [15], as well as its application to ultrastable AFM in ambient conditions [16]. We note that we did not optically stabilize the AFM in this present work, since the images were rapidly acquired.

In this instrument, two low-power (<1 mW) laser beams (λ = 810 nm and λ = 850 nm) were focused through a high numerical aperture (NA = 1.4) objective onto the surface. The back-scattered light from each focus was efficiently separated from the incoming light using an optical isolator formed by a polarizing beam splitter (PBS) and a quarter waveplate (λ/4), and detected using a quadrant photodiode (QPD). We actively minimized the intensity, pointing, mode, and polarization noise on each laser using a combination of optical elements in conjunction with active intensity stabilization. Furthermore, we offset amplified the total QPD signal, often referred to as the sum signal. Specifically, we subtracted a stable reference voltage V_0 from the original sum signal V_z and multiplied the resulting difference by a gain

#133107 - $15.00 USD Received 9 Aug 2010; revised 15 Oct 2010; accepted 26 Oct 2010; published 29 Oct 2010

(g) [*i.e.*, $g \cdot (V_z - V_0)$]. Cantilever deflection was observed using the standard optical lever laser (λ = 785nm, Fig. 2 (*red*)) [18]. Tip and sample motion were separately controlled using a pair of closed-loop 3D piezoelectric (PZT) stages (P363.3CD and P733.3DD, Physik Instrumente). The sample PZT stage was mounted on an ultrasonic substage (M-686.D64, Physik Instrumente), which was quiescent during AFM and optical imaging but allowed for coarse motion over large areas (10 × 10 cm^2) with 0.1-μm repeatability. Using this ability, we could image over large areas (~1 mm^2) by patching together 30 × 30 μm^2 fields (data not shown). Instrumentation control (LabVIEW 2009, National Instruments) used a data acquisition and control card containing a field-programmable gate array (PCIe-7852R, National Instruments).

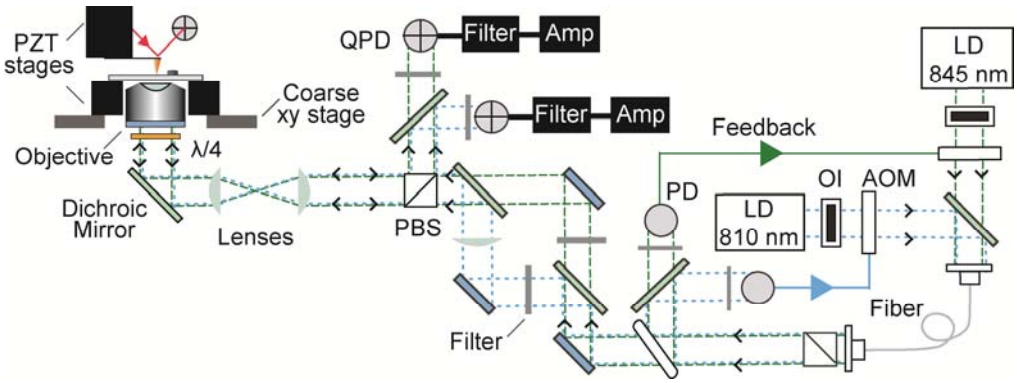

Fig. 2. Schematic of instrument. Beams from two laser diodes (LD, λ = 810, 845 nm) were actively stabilized to minimize noise using feedback to acousto-optic modulators (AOM) [17]. These stabilized beams were launched from a common polarization-maintaining fiber to minimize differential pointing noise. They were then separated by wavelength for independent steering. A lens in one beam path vertically shifted one of the foci in the imaging plane so as to simultaneously maximize the scattering signal from the tip and the fiducial mark on the surface. The beams were recombined, and a high numerical aperture objective focused them near the sample surface, where they scattered off of the tip or features on the substrate. Back-scattered light was efficiently separated using an optical isolator, formed by a quarter-wave plate (λ/4) and a polarizing beam splitter (PBS), and then collected onto quadrant photodiodes (QPD). The resulting signals were low-pass filtered with a cutoff frequency of 2.4 kHz for anti-aliasing purposes (Filter) and the sum signal was offset amplified (Amp). PD and OI denote photodiodes and optical isolators, respectively.

2.2 Sample preparation

The protocol for adsorption of patches of BR from *Halobacterium salinarum* (Sigma) was adapted from [19,20] for use on glass cover slips (Corning). The cover slips were cleaned by etching in 6M ethanolic KOH for 3 min. Silicon posts were added as fiducial marks via physical vapor deposition through a shadow mask [15]. Previous work from our group has shown that samples can be vertically aligned using a polystyrene bead stuck to the surface [15]. Although substrates with stuck beads are simpler to fabricate, we prefer silicon posts for AFM applications because the posts are uniformly distributed, preserve the surface chemistry, and are more stable. The cover slips were oxygen plasma treated for 4 min (PlasmaStar, Axic). Lyophilized BR was diluted to a stock concentration of ~250 μg/mL in 0.01% NaN_3. Immediately after the plasma cleaning, we applied 50 μL of adsorption buffer [300 mM KCl, 50 mM MgCl, 10 mM Tris HCl (pH 7.4)] onto the surface, then mixed in 20 μL of stock BR. After ~30 min incubation, the sample was rinsed with imaging buffer [300 mM KCl, 10 mM Tris HCl (pH 7.4)] and mounted in a liquid cell.

We note that light absorption inherent in BR was not the origin of our label-free imaging. BR-containing membrane is referred to as "purple membrane," due to its absorption

#133107 - $15.00 USD Received 9 Aug 2010; revised 15 Oct 2010; accepted 26 Oct 2010; published 29 Oct 2010

maximum at 568 nm that extends out to 650 nm [21]. Our imaging light (810 nm) was far detuned from this absorption.

2.3 Data collection and analysis

To optically image the sample, it was raster scanned through the focus by alternately moving the stage and collecting data. The back-scattered light was collected onto a QPD with a sensitivity of ~0.5 A/W at 810 nm (YAG 444-4A, Perkin-Elmer Optoelectronics) combined with a transimpedance amplifier with a gain of 100 kΩ. This signal was sent to custom low-noise electronics, designed and built in-house, that incorporated an offset amplifier. This offset amplification better matched the varying portion of the sum signal to the 20 V input range of the FPGA card used for data acquisition. For all data shown here, the gain was 100. We note that the gain could be increased significantly for label-free imaging, but was limited in this instrument to accommodate application to AFM stabilization [16]. Finally, we low-pass filtered the data at 2.4 kHz using a programmable multipole filter (Frequency Devices) and digitized at 5 kHz with a bit resolution of 0.3 mV. Each pixel in the optical images represents an average of 10 data points for a total observation period of 2 ms. During this process, the tip was retracted from the surface by ~2 mm, unless otherwise noted.

AFM images were acquired in constant-force contact mode at ~200 pN, using silicon nitride tips (OMCL TR-400, Oympus, $k_{\text{cantilever}} \approx 80$ pN/nm). The measured height of the purple membrane patches was ~8 nm. This value is consistent with prior reports of the height of purple membrane measured by AFM, which has been shown to range from 5 to 10 nm depending on ionic conditions and the substrate [22]. AFM images were flattened using software from Asylum Research.

2.4 Alignment

As a first step, we sequentially aligned the sample and then the tip to the pair of laser foci using the sample surface as the vertical reference ($z = 0$) (Fig. 3 (a)). Specifically, we scanned the silicon fiducial mark through the sample detection laser focus using the sample PZT stage and observed the position at which the signal was maximized. We then set the position of the sample to a predetermined offset from this maximum [15] ($\Delta z = 1.5$ µm for all data shown in this paper). Next, the vertical position of the tip was determined by touching the tip to the surface using the AFM PZT stage and then retracting it 60 nm. This protocol also yielded the sensitivity (V/nm) for the optical lever arm. We note that the laser foci are vertically offset by 2 µm to simultaneously maximize the scattering from the tip and the sample for application to ultrastable AFM [16]. If desired, a similar vertical alignment can be accomplished with a single laser.

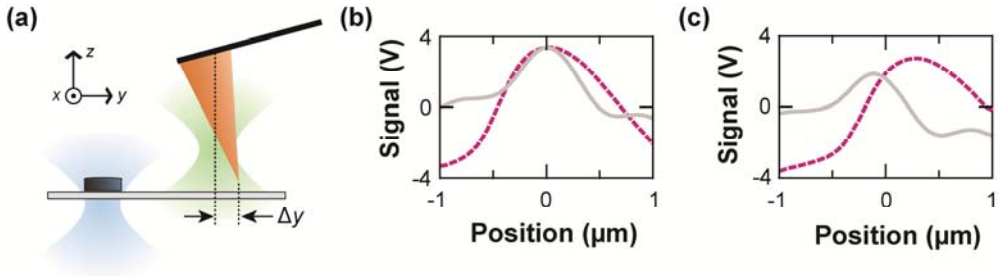

Fig. 3. Alignment of the tip to the optical axis of the laser (*green*) used for label-free imaging. (a) For increased precision, we aligned the position of the surface with respect to the laser foci by scattering a second laser beam (*blue*) off a silicon post. (b) The QPD sum signal as a function of tip position in *x* (*grey solid line*) and *y* (*purple dashed line*) aligned to maximize the sum signal. (c) The final alignment of the QPD sum signal as a function of lateral position after positioning to compensate for the fixed offset between the optical and the AFM image.

#133107 - $15.00 USD Received 9 Aug 2010; revised 15 Oct 2010; accepted 26 Oct 2010; published 29 Oct 2010

Next, we laterally aligned the tip to the optical axis of the tip-detection laser (Fig. 3(a), *green*). To do so, we sequentially scanned the tip along each lateral axis (Fig. 3(b)) and set the tip position to maximize the voltage along each line scan. We note that the precision of this alignment procedure (~10 nm) greatly exceeds the diffraction limit (~200 nm). We determined an offset (*e.g.*, Δy) between this empirically derived tip optical center and the tip's actual point of contact with the surface by comparing the position of the patch center using a two dimensional cross-correlation analysis (see Section 3.3). This offset was repeatable and remained constant for different tips of the same type, but varied between different types of tips. We measured an offset of 100 nm in *x* and 300 nm in *y* with an Olympus TR-400 tip tilted at 15° to the surface and aligned to a beam whose focus was approximately 500 nm above the surface. Finally, we incorporated this offset into the alignment procedure by positioning the tip away from the maximum of the optical signal (Fig. 3(c)).

3. Results

AFM studies of sparsely distributed biological structures would be accelerated by a tip-free, label-free means to find regions of interest. We first show that ~8-nm tall membrane patches were near the detection limit of optical imaging via back-scattered light, but offset amplification of the optical signal led to a 60-fold increase in the *S*/*N* (Section 3.1). The quality of the image was also enhanced (though to a lesser degree) by the presence of the AFM tip near the surface (~3 μm), but such images were altered along the cantilever's long axis (Section 3.2). Next, we show that these optical images could be registered to subsequent AFM images with nanometer-scale precision (Section 3.3). Finally, the lateral signals from the QPD rather than the sum signal can be used to highlight edges (Section 3.4).

3.1 Visualizing membrane patches with improved S/N

Nanometer-scale biological structures lead to small signals. The inherent back-scattered signal from ~8-nm tall patches of purple membrane with the tip far from the surface (shown schematically in Fig. 4(a)) yielded images with sufficiently low *S*/*N* that membrane patches were difficult to resolve (Fig. 4(b)). We quantified the signal by computing the normalized contrast $(I_{patch}- I_{glass})/I_{glass}$ between the on-patch signal (I_{patch}) and the off-patch signal (I_{glass}) [14]. The contrast from the membrane patches was 30-fold smaller than prior results on virons (45-nm dia.) [13]. The proposed contrast mechanism is an interference between back-scattered waves. Within this model, the expected normalized contrast for BR was estimated using a simple plane-wave model [23] with the appropriate index of refraction [24] and crystallographic height [25]. This estimate of 0.07% was consistent with the measured normalized signal of 0.06%. Thus, the low contrast was an inherent physical feature of the system and could not be increased for better image quality.

Therefore, we sought to improve *S/N* by decreasing noise. We note that the measured contrast is not inherently normalized: rather, the measured signal is a small modulation on top of a comparatively large signal, which is proportional to laser intensity (*I*). Hence, uncorrected fluctuations in *I* lead to noise in the image. But, in the images shown, the laser was actively stabilized ($\delta I/I$ <0.002% ; Δf = 0.02–100 Hz). Thus, fluctuations in *I* were not the origin of the low *S*/*N*.

On the other hand, the absolute change in the inherent signal was only 0.2 mV, smaller than the voltage change associated with a single bit [0.3 mV ($20\ V/2^{16}$)]. Thus, our image suffered from digitization noise. One solution would be to increase laser power, as has been done previously [14]. However, we sought a different solution for our AFM-based application, since even relatively small laser powers can lead to substantial deflection of the cantilever. Hence to minimize the perturbation to the tip and cantilever, we used a minimal laser power (~400 μW). An analogous problem exists in measuring the vertical motion of optically trapped beads with a detector laser sufficiently weak that it does not also act as a trap. In trapping, vertical bead motion also corresponds to the QPD sum signal and has

#133107 - $15.00 USD Received 9 Aug 2010; revised 15 Oct 2010; accepted 26 Oct 2010; published 29 Oct 2010

traditionally been limited to nanometer-sized measurements. Previous work from our lab has showed that the combination of intensity stabilization in conjunction with offset amplification allowed for significantly enhanced vertical sensitivity in comparison to intensity stabilization alone [17].

Using this same combination of techniques, single patches of purple membrane were well resolved (Fig. 4(c)). Quantitatively, the 100-fold gain used in the offset amplification led to a 60-fold increase in the *S*/*N*. From this improved image, we determined the lateral resolution of the optical images. Specifically, the rise in signal from the off-patch to on-patch region (10% to 90% of the signal) occurred over ~200 nm, consistent with prior work [14]. In this image, we also notice a faint line of unknown origin around the patch boundary.

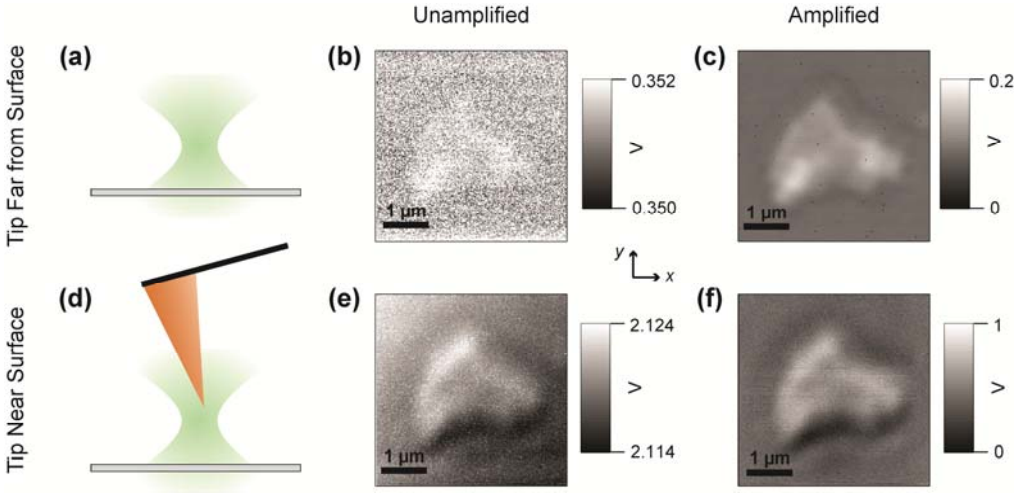

Fig. 4. Effects on the image of offset amplification and tip presence near the surface. When the tip was far (~2 mm) from the surface (a–c), the signal before amplification (b) was nearly lost in the noise, but the amplified image has *S/N* ≈20. Interestingly, with the tip near the surface (~3 µm, d–e), the membrane patch was clearly resolved even before amplification (e), though amplification still improved image quality (f). Both of these images show an asymmetric contrast along the *y*-axis – the long axis of the cantilever. Pixel spacing is 20 nm in all images. Amplified images were re-zeroed in post processing.

3.2 Enhanced optical image due to nearby AFM tip

The presence of an AFM tip retracted ~3 µm from the surface (shown schematically in Fig. 4(d)) enhanced the image formed from the unamplified signal (Fig. 4(e)). Given this micron-scale tip-sample separation, we note that this enhanced contrast is not consistent with a near-field effect. The presence of the tip also altered the nature of the contrast along the long axis of the cantilever, producing an asymmetric edge effect qualitatively similar to DIC images. Offset amplification further enhanced this image (Fig. 4(f)). Note that there is a 5-fold increase in the voltage range between Figs. 4(b) and 4(e), and between Figs. 4(c) and 4(f). While further work is needed to understand the origin of this enhanced contrast, optical imaging with the tip in the vicinity of the surface could be valuable for three reasons. First, this enhanced contrast obviates the need for offset amplification for imaging membrane patches. Second, coarse motion of the tip (outside the 5-µm range of the PZT stage) is not required between acquisition of the optical and AFM image. Finally, tip-enhanced contrast suggests a means to image even smaller label-free biological structures via back-scattered, far-field optical imaging.

#133107 - $15.00 USD Received 9 Aug 2010; revised 15 Oct 2010; accepted 26 Oct 2010; published 29 Oct 2010

3.3 AFM image inherently spatially registered to optical image

These label-free optical images were inherently registered to AFM images, because the tip was aligned with the optical axis of the imaging beam. Initially, there was a lateral offset between the optical image (Fig. 5(a)) and the AFM image (Fig. 5(b)). This offset was due to the difference between the optical center of the tip and the tip's point of contact with the sample. As discussed above, the optical center of the tip was determined through a routine that maximized the signal from the back-scattered light (Fig. 3(b)). We note that such scattering most likely occurred from the body of the tip near the focus rather than the true apex of the tip. Indeed, measurements showed that the geometry of the tip and the vertical height above the surface affected this offset. We would also expect it to be dependent on the tilt of the cantilever. By cross-correlating these two images (Fig. 5(c)), we measured an offset of 100 nm in *x* and 300 nm in *y* (Fig. 4 (c)). Once this offset was determined, it was eliminated in future image acquisition by compensating the alignment of the tip relative to the optical axis, as shown in Fig. 3(c).

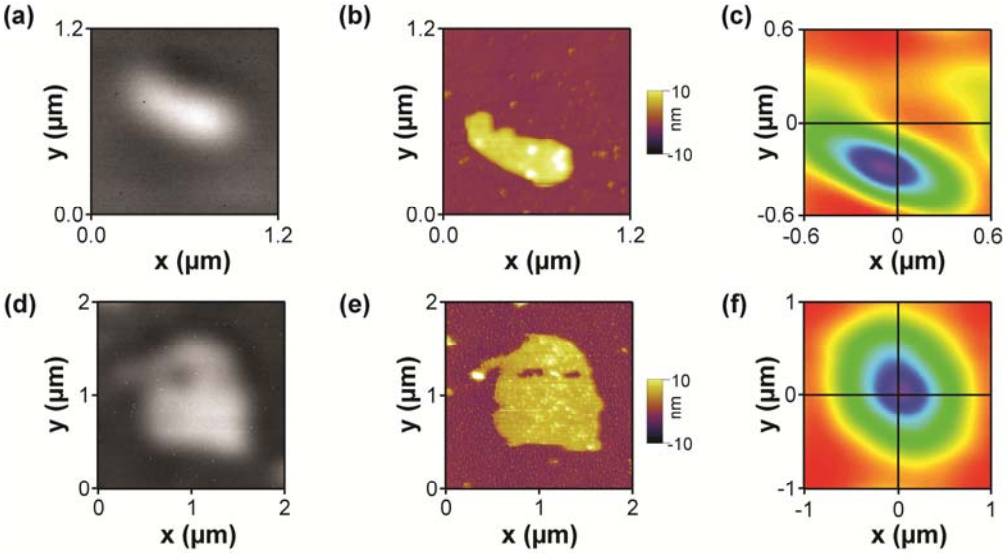

Fig. 5. Spatial registration between optical and AFM images. When the tip is positioned at its optical center, an optical image (a) and AFM image (b) of the same region show the same feature, but with an offset. (c) Cross-correlation analysis was used to quantify this offset to be 100 nm in *x* and 300 nm in *y*. After centering the tip to account for this effect, an AFM image (d) and an optical image (e) of the same area. Cross-correlation analysis (f) showed nanoscale alignment of the two images (40 nm in *x* and 30 nm in *y*). Pixel size was 4 nm and 10 nm in the AFM and optical images, respectively.

The geometric origin of this offset suggests that it should be constant over time. To test this idea, we acquired a new set of optical and AFM images (Fig. 5(d–e)). The cross-correlation analysis (Fig. 5(f)) revealed a nanoscale alignment between the two images (40 nm in *x*; 30 nm in *y*). Note that the second set of images was acquired with a different tip on a different sample two weeks after the lateral offset was originally determined. Thus, the nanoscale registration and alignment between the label-free image and the subsequent AFM was robust and repeatable.

3.4 Enhanced edge signals using the lateral signals from the QPD

For completeness, we note that a QPD provides for lateral signals (*e.g.*, the difference between the left and right halves) in addition to the sum of all light falling on the detector (Fig. 6(a)). The images from these lateral signals enhanced the edges of features (Fig. 6(b–c)),

#133107 - $15.00 USD Received 9 Aug 2010; revised 15 Oct 2010; accepted 26 Oct 2010; published 29 Oct 2010

again reminiscent of images taken with DIC. Future work may be able integrate these lateral signals with the sum signal to allow for better feature extraction or detection of smaller objects.

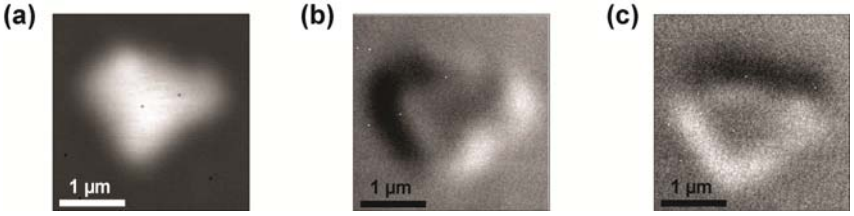

Fig. 6. Edges highlighted on the *x* and *y* channels of the QPD. (a) The sum signal. (b) The signal from the *x* channel highlights the left and right edges of the feature. (c) Similarly, the signal from the *y* channel highlights the top and bottom edges of the feature.

4. Conclusion

By enhancing a new label-free imaging technique [13,14], we successfully produced images of biological assemblies that had an inherent contrast 1/30th of those imaged in prior work [13]. In spite of this low inherent contrast from individual membrane patches, the resulting images had an excellent *S/N* of 20. Given the high *S/N* in these images, we expect label-free imaging to be successful for protein assemblies that are smaller or have a lower inherent contrast. We further showed enhanced contrast when the tip was near the surface, a fact that could be exploited to image even smaller objects. Further exploration of the physical origin of this effect could lead to interesting findings and improvements in this label-free optical imaging. From a practical perspective, the simplicity and non-destructive nature of optical imaging enables us to assess the cleanliness and overall quality of samples over very large areas.

The registration and alignment of the optical image with the AFM image allows us to optically locate the sparsely distributed patches without unwanted degradation to the tip or the sample. This nanometer-scale alignment arose from the static offset between the tip's optical center and its point of contact with the surface. Importantly, this offset was constant, allowing a single offset value to be used for multiple tips of the same type over several weeks. Locating regions of interest by optical scanning can increase throughput of data collection, often a limiting factor in single-molecule studies. For force spectroscopy and other manipulation processes, it bypasses the need to image with the tip, opening up new possibilities for high-strength covalent attachment between the tip and the sample under study. For instance, the tip can be deterministically brought down onto either a clean region of the surface or a membrane patch without prior AFM imaging. Thus, we expect the combination of label-free optical imaging with AFM to be a valuable addition to biological AFM.

Acknowledgements

The authors acknowledge Louisa Eberle and Duc Nguyen for assistance. This work was supported by an NIH Molecular Biophysics Training Scholarship (ABC, T32 GM-065103), a Burroughs Wellcome Fund Career Award at the Scientific Interface (GMK), a Butcher Grant, the National Science Foundation (DBI-0923544, Phy-0551010) and NIST. Mention of commercial products is for information only; it does not imply NIST's recommendation or endorsement. T. T. Perkins is a staff member of NIST's Quantum Physics Division.

#133107 - $15.00 USD Received 9 Aug 2010; revised 15 Oct 2010; accepted 26 Oct 2010; published 29 Oct 2010